Available online at www.sciencedirect.com

ScienceDirect

Ceramics International 40 (2014) 4193–4201

CERAMICS INTERNATIONAL

www.elsevier.com/locate/ceramint

Application of the statistical Taguchi method to optimize TiO_2 nanoparticles synthesis by the hydrothermal assisted sol–gel technique

Sanaz Naghibi[a,*], Mohammad Ali Faghihi Sani[b], Hamid Reza Madaah Hosseini[b]

[a]Department of Materials Engineering, Science and Research Branch, Islamic Azad University, P.O. Box: 14778-93855, Tehran, Iran
[b]Department of Materials Science and Engineering, Sharif University of Technology, P.O. Box: 11155-9466, Tehran, Iran

Received 7 July 2013; received in revised form 15 August 2013; accepted 18 August 2013
Available online 26 August 2013

Abstract

TiO_2 nanoparticles were synthesized by hydrothermal assisted sol–gel technique. The preparation parameters including pH value, the amount of water, titanium tetra isopropoxide content, temperature and time of hydrothermal process were investigated by Taguchi statistical experiments to determine the influence of synthesizing variables on the optimal conditions and to realize the highest degree of crystallinity or smallest crystallite size. X-ray diffraction (XRD) analysis and direct band gap energy (E_g) values, measured via diffuse reflectance spectra (DRS), proved that all the samples consist of anatase as a unique phase. Transmission electron microscopy (TEM) and specific surface area values showed that the sample with the smallest crystallite size could exert more effective photoactivity confirmed by measuring the decomposition rate of methylene blue. The apparent photodegradation rate constant of the sample with the smallest crystallite size was about five times greater than that of commercial TiO_2.

A higher photoactivation performance of TiO_2 nanoparticles could be achieved using 45 mL of water and 3.79 mL of titanium tetra isopropoxide in a sol with pH of 9 and passing hydrothermal process at 100 °C for 18 h.

Keywords: TiO_2 nanoparticle; Hydrothermal assisted sol–gel technique; Taguchi method; Photocatalytic activity

1. Introduction

Excellent biocompatibility [1,2], high chemical stability [3] and unique photocatalytic properties [4] provided by TiO_2 nanoparticles (NPs) make it a remarkable candidate for the vast number of applications [5] in the efficient delivery of therapeutic and diagnostic agents [6,7], sonodynamic therapy [8], permanent anti-corrosion coating [9], solar cells [10] and etceteras. Photocatalytic property of TiO_2 is being extensively utilized to rectify a variety of environmental pollution problems such as decomposition of unwanted and toxic organic compounds, degradation of pollutants from contaminated water and air by killing harmful bacteria [11–15] and cancer cells [16–19].

Some recent studies have focused on synthesizing TiO_2 NPs to improve their photocatalytic properties [20–24]. In comparison to brookite and rutile, the anatase phase is the most attractive choice for photodegradation due to its enhanced photoactivity [3]. On the other hand, the photocatalytic activity of TiO_2 is strongly facilitated by raising the degree of crystallinity and specific surface area of NPs [25]. In this regard, the hydrothermal assisted sol–gel synthesis method could be an appropriate candidate for preparation of a well-crystalline and narrow particle size distribution. This route provides lower temperature synthesis than solid-state reactions and utilizes heat and pressure to initiate reactions of reagents dissolved in water. This opens up reaction chemistry which is not accessible under ambient conditions, and crystalline NPs can be produced without the need of post reaction calcinations, and with minimal or no agglomeration [26,27].

*Corresponding author. Tel.: +98 21 47911; fax: +98 21 44868474.
E-mail addresses: naghibi@iaush.ac.ir, sanaz_n77@yahoo.com (S. Naghibi), faghihi@sharif.ir (M.A. Faghihi Sani), madaah@sharif.ir (H.R. Madaah Hosseini).

0272-8842/$ - see front matter © 2013 Elsevier Ltd and Techna Group S.r.l. All rights reserved.
http://dx.doi.org/10.1016/j.ceramint.2013.08.077

Taguchi method is a very useful tool to solve the complex and confusing problems with fewest variables and fewer tests in many areas. It uses an orthogonal arrays to determine the effect of the variables on characteristic properties, and to optimize conditions of selected variables [28,29]. This statistical method was successfully utilized to optimize the preparation condition of ceramic materials which have been reported elsewhere [9,30].

In this study, Taguchi method was used to determine the best TiO_2 NPs preparation conditions (to approach the highest degree of crystallinity or the smallest particles size). The surveyed variables included the pH value of suspension, the amount of water, titanium precursor content, the temperature and time of hydrothermal process.

2. Experimental procedure

2.1. Experimental design

In this study, a standard Taguchi experimental plan with notation L_{16} (1024) was chosen to optimize experimental conditions to evaluate the degree of crystallinity or the crystallite size of NPs prepared by hydrothermal assisted sol–gel technique under various preparation parameters (i.e. pH value, the amount of water, titanium tetra isopropoxide (TTIP) content, temperature and time of hydrothermal process). To find the optimum preparation conditions, the input parameters (four variables in four levels) were chosen as presented in Tables 1 and 2.

Based on the Taguchi method, the optimization of observed values was determined by comparing the mean of means values.

2.2. Starting materials

The starting materials were TTIP ($>98\%$), isopropyl alcohol (iPrOH, $>99.5\%$), hydrochloric acid (HCl, 37%) and triethylamine (TEA, $>99\%$) (all from Merck®, Frankfurt, Germany). Commercial TiO_2 samples (trade name: AEROXIDE® TiO_2 P25, average particle size: 21 nm, specific surface area: 50 ± 15 m^2/g, purity: $>99.50\%$, contains mixed anatase and rutile, from Degussa®, Evonik, Essen, Germany), were also used as reference materials for comparison.

2.3. Preparation of TiO_2 NPs

According to Table 2, NPs were prepared by using TTIP as a Ti source, iPrOH as a solvent, HCl as a reagent to adjust pH and distilled water as a hydrolytic agent. It was known that in Ti^{4+} containing sol, the hydrolysis does not occur in pH more than 1.75 [31]. Therefore, to decrease pH value to 1.5, HCl was added to the solutions. Then, they were continuously stirred for 48 h. In this step, adequate amounts of TEA were dropped to the solutions to make the pH reach the respected values (7, 9, 10 and 11, according to Table 2). The obtained

Table 1
Parameters and levels that used for the experimental design in the hydrothermal assisted sol–gel process.

Factors	pH	V_{water} (mL)	V_{TTIP} (mL)	T (ºC)	Time (h)
Levels	7	36	3.79	100	8
	9	40.5	5.05	130	12
	10	45	7.58	160	18
	11	54	15.17	200	24

Table 2
Compositions and conditions of the samples on the basis of $L_{16}(4^5)$ orthogonal array in the Taguchi method.

Code	pH	V_{water} (mL)	V_{TTIP} (mL)	T (°C)	Time (h)
1	7	36	3.79	100	8
2	7	40.5	5.05	130	12
3	7	45	7.58	160	18
4	7	54	15.17	200	24
5	9	36	5.05	160	24
6	9	40.5	3.79	200	18
7	9	45	15.17	100	12
8	9	54	7.58	130	8
9	11	36	7.58	200	12
10	11	40.5	15.17	160	8
11	11	45	3.79	130	24
12	11	54	5.05	100	18
13	10	36	15.17	130	18
14	10	40.5	7.58	100	24
15	10	45	5.05	200	8
16	10	54	3.79	160	12

white precipitate suspensions were then placed in a Teflon recipient inside of a stainless steel autoclave. Hydrothermal treatment was performed in different conditions according to Table 2. The prepared precipitates after filtering and repeatedly washing (3 times with distilled water) were then dried at 70 °C for 24 h.

2.4. Characterization

XRD analysis was done by an XRD (D8 advance, Bruker, Germany) using Cu tube anode (Kα = 1.540598) and Ni filter. PANalytical X'Pert HighScore software was also used for the analysis of different peaks. The diffraction patterns of products were compared to propose Standards by the Joint Committee on Powder Diffraction and Standards (JCPDS).

Crystallite sizes of specimens were calculated from broadening of XRD peaks using the Williamson–Hall method [32] according to

$$B\cos\theta = (0.9\lambda/d) + \eta\sin\theta \quad (1)$$

where d, θ, λ, η and B are the crystallite size, diffraction angle, wavelength of the X-ray ($\lambda_{Cu k\alpha 1} = 1.540598$ Å), lattice strain and the peak full width at half maximum (FWHM), respectively. Thus, when "$B\cos\theta$" is plotted against "$\sin\theta$" (for main peaks of each XRD patterns), a straight line is obtained with the slope as (η) and the intercept as ($0.9\lambda/d$).

The crystallite size and qualitatively assess strain based upon peak broadening could be calculated according to the drawn diagram.

The degree of crystallinity of TiO_2 NPs was quantitatively evaluated. In this method, 'sum of net area'/'sum of total area' in PANalytical X'Pert HighScore software was the criterion for the degrees of crystallinity. To calibrate the results, backgrounds of peaks were determined by considering 100% crystallinity for the commercial TiO_2–P25.

DRS were obtained by a UV–vis. scanning spectrophotometer (V-670, 195–600 nm, Jasco®, Tokyo, Japan). E_g of the samples was calculated based on a plot of $(\alpha h\nu)^2$ against the photon energy $h\nu$ (where α is the absorption coefficient) and by extrapolating the linear part of the curve to $(\alpha h\nu)^2 = 0$ [25].

The selected samples were also studied by using a TEM (Philips®, Amsterdam, Netherlands). The microscope was operating at an accelerating voltage of 100 kV. Samples were prepared by dipping a Cu grid into ultrasonic dispersion of the oxide powder in ethanol.

The specific surface area values were computed from the adsorption isotherms using the Brunauer–Emmett–Teller (BET) method. The adsorbate used was N_2 and the isotherms were recorded at 77 K using an adsorption apparatus (Belsorp mini II, BEL Japan Inc., Osaka, Japan).

The photocatalytic activities of the samples were evaluated by measuring the decomposition rate of methylene blue at room temperature and comparing the results with the activity of TiO_2–P25. In each experiment, a suspension containing 100 mg of catalyst and 100 mL of aqueous methylene blue solution (30 mg/L) was continuously stirred in a glass flask and irradiated with 365 nm UV lamp (2 × 15 W, Philips). The distance between the light source and the surface of the suspension was 10 cm and the sample area for testing was fixed at 40 cm^2. The irradiated solution was centrifuged to separate NPs. Then, the changes of methylene blue concentration versus time were measured by a UV–vis spectrophotometer at 664 nm with a 30 min interval for a total irradiation time of 90 min. The degradation rates (k, min^{-1}) were measured from the slops of $\ln(C_0/C)$ versus irradiation time (t) curves at the first 30 min of reaction and presuming a first order kinetics at this stage of the reaction (where C_0 and C are the concentrations of methylene blue at the initial time and at the time, t, respectively).

3. Results and discussion

3.1. Optimization of process parameters to minimize crystallite size or maximize crystallinity

Fig. 1 shows XRD patterns of the powders prepared by the hydrothermal assisted sol–gel synthesis method. All the samples consist of anatase as a unique phase (JCPDS no. 78-2486). No crystalline phase ascribed to rutile or brookite could be found.

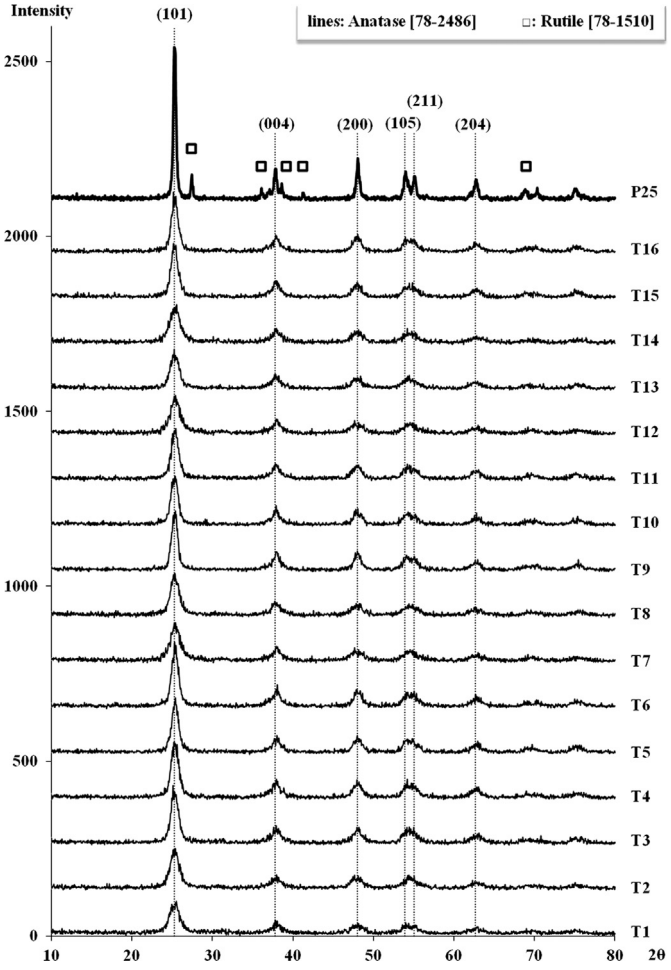

Fig. 1. XRD patterns of TiO_2 synthesized samples.

E_g values of all samples were calculated based on the DRS results and reported in Table 3. All the samples showed similar absorption spectra with absorption edges around 400 nm. E_g values ranged between 3.21 and 3.28 eV those are closed to that of anatase (3.26 eV) [3] has good agreement with the results of XRD.

Table 3
Crystallite size, degree of crystallinity and E_g of samples and TiO_2–P25.

Code of samples	Crystallite size (nm) from XRD	Crystallinity (%) from XRD	E_g (eV) from DRS
TiO_2–P25	21	100	–
1	9.8	62	3.21
2	16	75	3.25
3	3.9	94	3.26
4	10.6	95	3.26
5	16.9	96	3.25
6	9.3	98	3.25
7	5	74	3.22
8	7.9	76	3.25
9	9.2	85	3.28
10	18	90	3.24
11	12.3	97	3.25
12	7.8	67	3.24
13	7.4	75	3.24
14	17	77	3.23
15	12.4	96	3.25
16	16.7	90	3.27

The crystallite size and relative anatase crystallinity of samples are shown in Table 3. In order to confirm the crystallite size values estimated from XRD patterns, the particle sizes of the selected samples were calculated from TEM images.

TEM images of the selected synthesized samples (3, 5 and 6) and TiO_2–P25 are shown in Fig. 2. As can be seen powders have semi-spherical or cubic shapes with a narrow particle size distribution (~2–12 nm), while TiO_2–P25 has a broad particle size distribution (~4–36 nm). These results confirm the crystallite size calculated by XRD results.

According to the numerical data in Table 3 and based on the Taguchi method, using an L_{16} orthogonal array, the influence of the sample design parameters on the degree of crystallinity and crystallite size are shown in Fig. 3. As can be seen, time and temperature have the greatest influence on the final sample crystallite size and crystallinity, respectively. By increasing the hydrothermal time and temperature, crystallite size is increased due to Ostwald ripening phenomenon [21,24,25]. However, in this work, by increasing the temperature, the crystallite size was first increased to a maximum value and then decreased. This trend was reversed by increasing time. It could be noticed that the grain growth of NPs is influenced by the nucleation rate and driving force together. At first, the formation of small

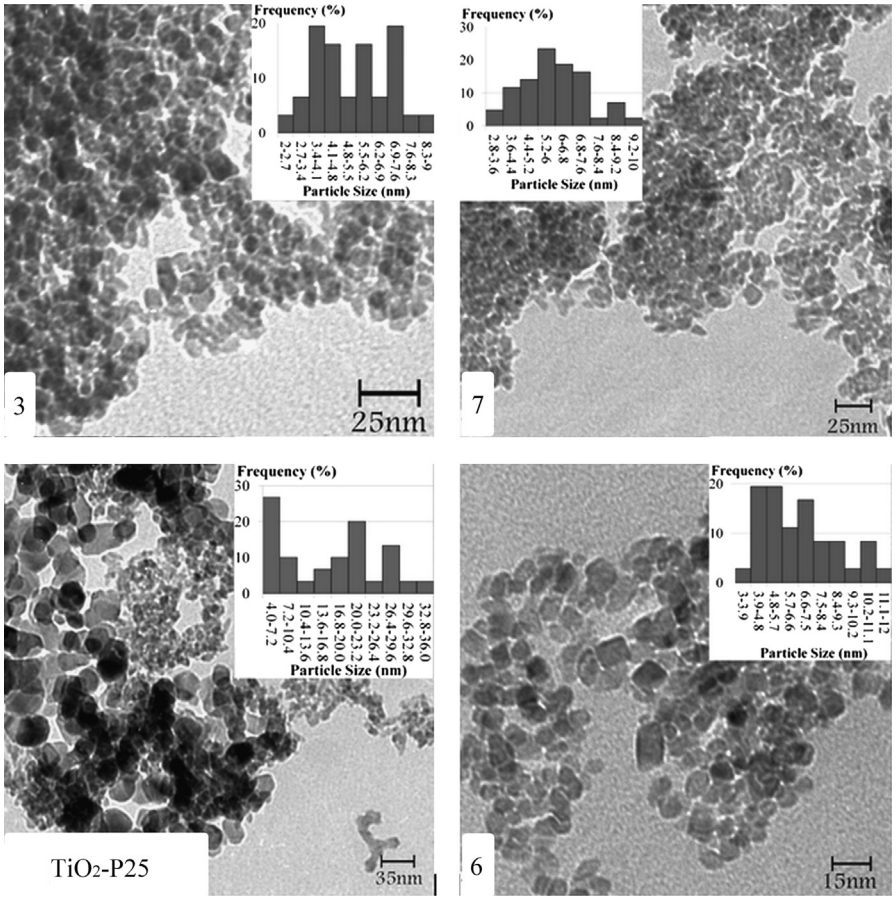

Fig. 2. TEM images of various TiO_2 samples and their particle size distribution histograms.

crystalline nuclei in a supersaturated medium happens and these tiny nuclei begin to grow up. The primary driving force for the crystal growth in this stage is the reduction in surface energy [33]. As the temperature increased from 160 to 200 °C, crystallite size decreased due to the partial dissolution of as-crystallized NPs at high pressure under hydrothermal conditions [34].

According to Fig. 3, by increasing in hydrothermal time, the crystallite size was decreased to a minimum value and then increased. In this case, increasing the hydrothermal time caused to the more solubility of the formed crystallites and decreased crystallite size [34]. When the hydrothermal time increased from 18 to 24 h, the crystallite size increased because of the reduction in surface energy as driving force for grain growth.

When the amount of TTIP increased, crystallite size diminished (Fig. 3) because of faster nucleation rate of TiO_2 compared to the crystal growth [35].

According to the literatures [21,36], the absence of water during the solvothermal reaction retards the crystallization and grain growth of TiO_2 NPs. By increasing the amount of water, hydrolysis of precursor and phase transformation from amorphous to anatase and grain growth are enhanced. Higher amount of water performs as a diluent for precursor suspension, increasing the diffusion distance and decreasing the crystallite size. Furthermore water has no effect on crystallite size sensibly.

Moreover, by increasing pH value, crystallite size of TiO_2 NPs was increased. As reported by Sugimoto et al. [37], when the pH increases from 9 to 10, the only present Ti hydroxide is $Ti(OH)_4$ and there are no other complexes such as $Ti(OH)_3^+$, $Ti(OH)_2^{2+}$ or $Ti(OH)^{3+}$. By increasing pH, the condensation and polymerization process come about and crystallite growth of NPs happens due to the aggregation of condensed species [38].

As shown in Fig. 3, the crystallinity raised with an increase in hydrothermal time and temperature due to Ostwald ripening phenomenon which is in accordance with the results reported in literatures [21,25,39,40].

As can be seen in Fig. 3, by increasing the amount of TTIP, the crystallinity of NPs decreased and then, no significant change observed. This may be attributed to the fact that TTIP addition and hence the decrease in the crystallite size result in approaching NPs to amorphous phase and consequently their crystallinity is diminished.

As found by other researchers [21], at high water content, the rate of hydrolysis reaction is relatively high. Decreasing the water volume in hydrothermal process increases the amount of unhydrolyzed alkyls leading to a decrease in the degree of crystallinity by adsorbing alkyls on the surfaces of as-crystallized TiO_2 NPs.

By increasing the amount of pH, because of completing hydrolysis reaction, phase transformation of amorphous to anatase is accelerated and the crystallinity is increased.

Photocatalytic properties of NPs depend on their crystallinity and/or crystallite size [25]; therefore, specification of preparation condition to synthesize NPs with the highest degree of crystallinity or the lowest crystallite size was determined as the aim of this section. To achieve this goal by optimizing the composition of the starting mixtures and other processing parameters by the statistical Taguchi method, the processing factors that exert the greatest effects were summarized in Table 4. Based on these results, two samples were designed, expecting to lead to the formation of TiO_2 anatase NPs with the highest degree of crystallinity (HDC) or TiO_2 anatase NPs with the smallest crystallite size (SCS). For this reason, these samples were prepared and characterized as below.

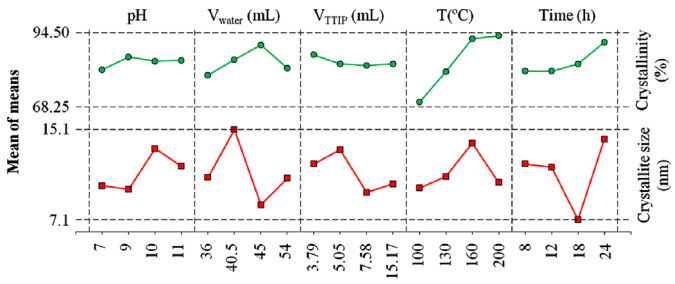

Fig. 3. Influence of design parameters on the crystallite size and crystallinity of the samples.

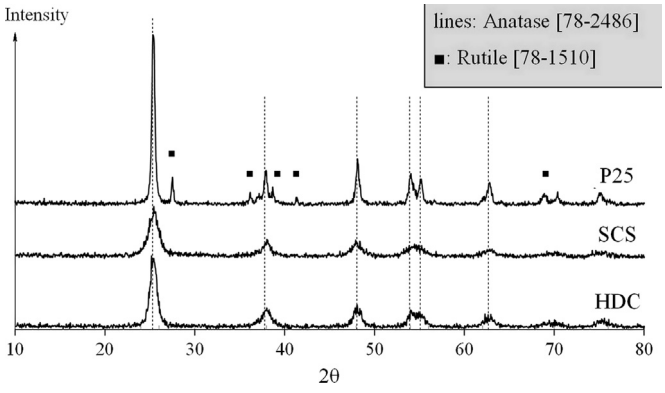

Fig. 4. XRD patterns of HDC and SCS samples.

Table 4
Summary of optimum configurations for HDC and SCS samples.

Samples	pH	V_{water} (mL)	V_{TTIP} (mL)	T (°C)	Time (h)
HDC	9	45	3.79	200	24
SCS	9	45	7.58	100	18

3.2. Investigation on behavior of the optimized NPs (HDC and SCS)

Fig. 4 shows XRD patterns of HDC and SCS samples confirming the formation of anatase as a unique phase. The results of DRS (Fig. 5) and calculated E_g values (Table 5) support the XRD results. E_g values of HDC and SCS are 3.27 and 3.23 (Table 5), respectively, which are in a good agreement with those of plain anatase, 3.26 eV [3].

Table 5 shows the crystallinity values and crystallite sizes of these samples. As can be seen in Tables 3 and 5, the optimum conditions for the crystallinity and crystallite sizes were authentic because the crystallinity of HDC (99%) was higher and crystallite size of SCS (3.5 nm) was lower than those of other samples. These results show that the Taguchi analysis is suitable for optimizing a range of preparation parameters and that the optimized conditions can be used as the basis for further development. All parameters enhancing the degree of crystallinity have been summarized in sample HDC; therefore, its increase in crystallinity is justifiable and so is the case of SCS.

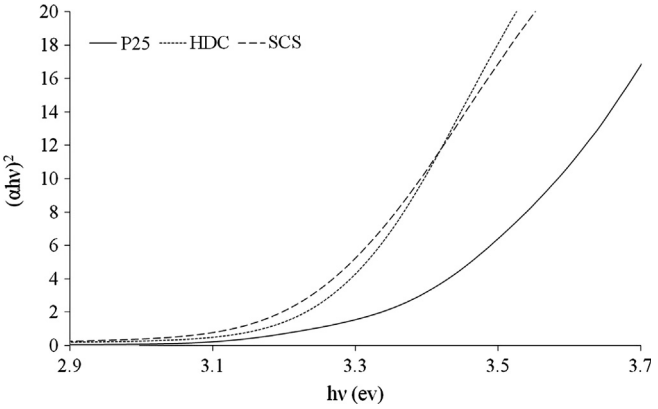

Fig. 5. DRS results for HDC, SCS and P25 samples.

Table 5
Crystallite size, crystallinity and E_g of HDC and SCS samples.

Code	Crystallite size (nm)	Crystallinity (%)	E_g (eV)
THC	8	99%	3.27
SCS	3.5	83%	3.23

Photocatalytic activity measuring, TEM and BET analysis were utilized for comparing HDC and SCS.

TEM images of samples HDC and SCS in Fig. 6 reveal that distinct irregularly spherical particles with a narrow size distribution ranging from 5 to 14 nm and 3 to 8 nm, respectively, with few rod-like crystals in sample SCS. The growth of anatase NPs in hydrothermal process happens via four stages. In the first stage, small uni-dimensional anatase nanocrystals with zigzag surfaces form and grow. In the second stage, anatase nanocrystals grow abruptly along [001] direction. The third growth stage shows an acceleration along [101] direction and a retardation along [001] direction, so that the diameter along [001] direction becomes equal to that along [101] direction. In the final growth stage, the diameter along [001] direction grows more rapidly than that along [101] direction [41]. According to these phenomena, SCS is in the first growth stage because of lower hydrothermal time and temperature, forming rod-like crystals. Unlike other samples, HDC lays in the third growth stage due to the highest temperature and time during hydrothermal process, and hence spherical particles were synthesized. The specific surface area of particles is affected by their feature such that there is a minimum in the sphere shape. It is expected that SCS exerts higher photoactivity due to its higher specific surface area; therefore, to evaluate this, BET analysis was utilized.

Nitrogen adsorption–desorption isotherms and Barret–Joyner–Halenda (BJH) pore size distribution plots of HDC and SCS samples together with those of TiO_2–P25 are illustrated in Fig. 7 and Table 6. These curves present type IV isotherms which indicate that the samples contain mesoporous structures [24]. Formation of mesoporous structures for these samples is attributed to the aggregation of TiO_2 NPs. This phenomenon can be explained by fact that long range ordered mesoporous structure were not detected in TEM images (Figs. 2 and 6), therefore it can be concluded that the mesoporosity of these samples is basically caused by the interparticle porosity rather

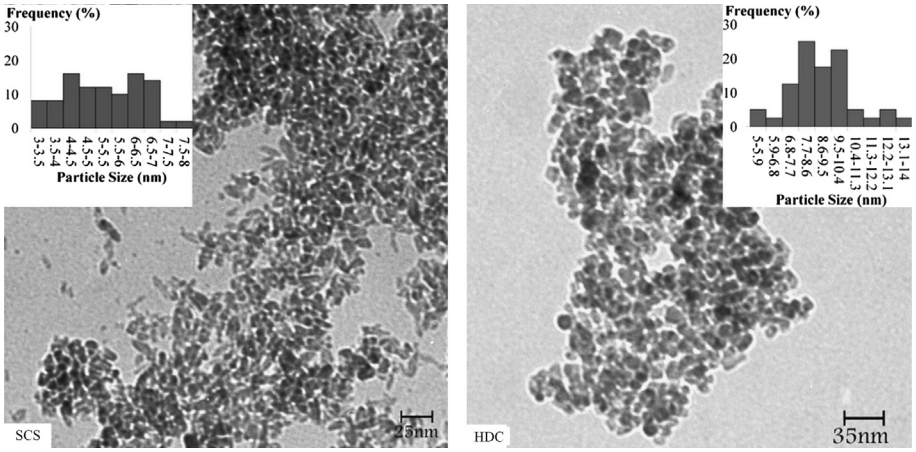

Fig. 6. TEM images of SCS and HDC samples and their particle size distribution histograms.

than intraparticle porosity. Broad pore size distribution of HDC sample may be ascribed to the disordered aggregation of TiO_2 NPs at higher hydrothermal time and temperature [24]. The amount of TTIP in SCS sample is higher than that of HDC sample. By increasing the molar fraction of Ti ions, the hysteresis loops shift toward smaller relative pressures and the areas of the hysteresis loops become bigger [22]. It can be observed that due to the higher hydrothermal time and temperature, and consequently larger crystallite size in the HDC sample, it has smaller specific surface area and larger mean pore size in comparison to the SCS sample. This result confirms the TEM investigation suggesting that SCS could improve photoactivity in comparison to HDC.

Finally, to choose one sample as the best, the photocatalytic activities of HDC and SCS were evaluated. The photocatalytic activities of the obtained NPs and TiO_2–P25 were assessed by degradation of methylene blue solution under UV irradiation. Fig. 8 shows the $\ln(C_0/C)$ versus irradiation time (t) curves and the degradation rates were illustrated in its inset. This figure shows that the first order kinetic of dye removal kinetic is acceptable for both samples (SCS and HDC), but comparison of the lines slop show that $k_{SCS} > > k_{P25} > k_{HDC}$. Photocatalytic activity of anatase TiO_2 NPs is severely affected by the crystallite size, surface area, and pore structure. Smaller crystallite size, higher surface area and larger pore volume are noted to have positive effects on the photocatalytic activity [24]. Despite the lower pore volume of SCS sample (Table 6), it indicated the most photocatalytic activity. This fact can be related to the smaller crystallite size (Table 5) and the higher specific surface area (Table 6). k_{SCS} is about five times greater than that of TiO_2–P25. These results are confirmed by XRD, TEM and BET analysis.

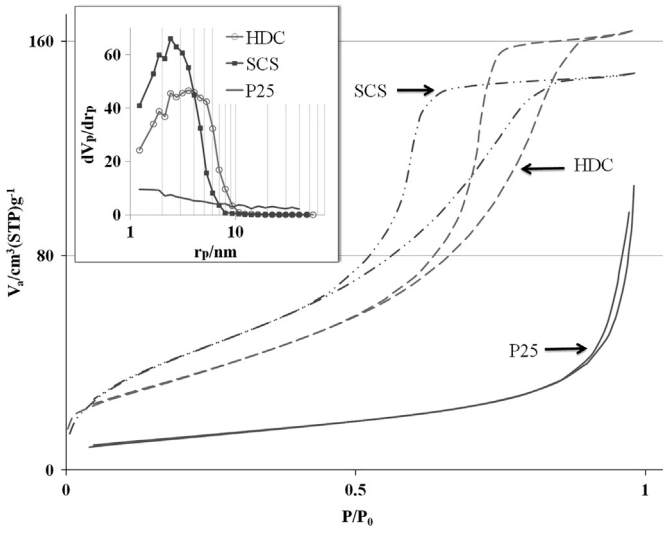

Fig. 7. Nitrogen adsorption–desorption isotherms and BJH pore size distribution plots (inset) of HDC, SCS and P25 samples.

Table 6
Numeral results of BET and BJH of TiO_2–P25, HDC and SCS samples.

Code	S_{BET} (m^2/g)	Mean pore size (nm)	Total pore volume (cm^3/g)
HDC	125	8.1042	0.2540
SCS	160	5.7198	0.2290
P25	43	15.244	0.1639

4. Conclusion

Anatase TiO_2 NPs can be synthesized by a hydrothermal assisted sol–gel technique with particle size distribution in the range of 2–12 nm. The results of the Taguchi method showed that time and temperature had the greatest influence on the final sample crystallite size and crystallinity, respectively.

Due to the effects of crystallinity and crystallite size on photoactivation of NPs and based on the results of the Taguchi method, HDC and SCS samples were prepared. BET results showed that due to the lower hydrothermal time and temperature and consequently, smaller crystallite size in the SCS sample, it has greater specific surface area and smaller mean pore size in comparison to HDC sample.

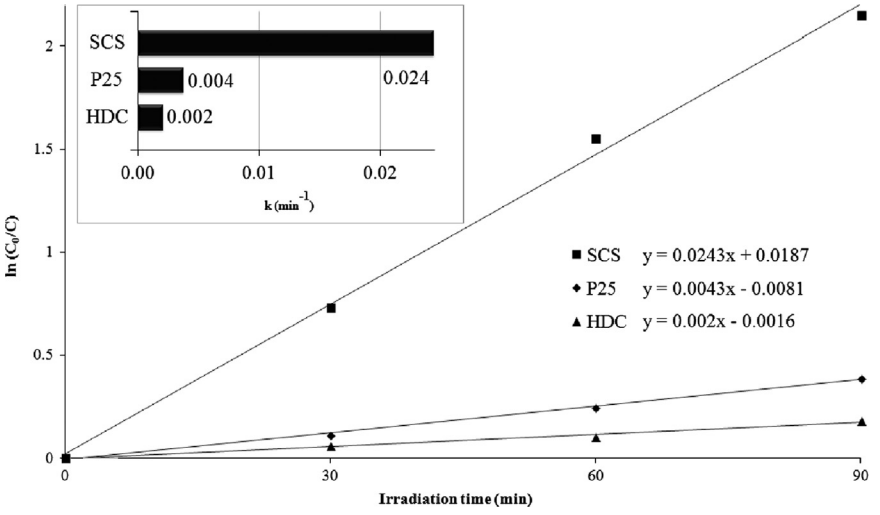

Fig. 8. Kinetics of the photocatalytic degradation of methylene blue solutions containing (■) SCS, (▲) HDC and (◆) TiO_2–P25. The apparent rate constants (k, min^{-1}) of degradation of methylene blue were illustrated in the inset.

Based on the results of photodegradation, SCS had the most photocatalytic activity and its apparent rate constant was about five times greater than that of TiO_2–P25.

The optimum processing conditions to achieve the goal of this research, namely a highly photoactive TiO_2 NPs, were found to be: $V_{H_2O}=45$ mL, $V_{TTIP}=3.79$ mL, pH=9, $T_{\text{hydrothermal process}}=100\ ^{\circ}C$ and $t_{\text{hydrothermal process}}=18$ h.

References

[1] W. Han, Y. Wang, Y. Zheng, In vivo biocompatibility studies of nano TiO_2 materials, Advances in Materials Research 79–82 (2009) 389–392.

[2] W. Han, Y. Wang, Y. Zheng, In vitro biocompatibility study of nano TiO_2 materials, Advances in Materials Research 47–50 (2008) 1438–1441.

[3] O. Carp, C.L. Huisman, A. Reller, Photoinduced reactivity of titanium dioxide, Progress in Solid State Chemistry 32 (2004) 33–177.

[4] K. Hashimoto, H. Irie, A. Fujishima, TiO_2 photocatalysis: a historical overview and future prospects, Japanese Journal of Applied Physics 44 (2005) 8269–8285.

[5] X. Chen, S.S. Mao, Titanium dioxide nanomaterials: synthesis, properties, modifications, and applications, Chemical Reviews 107 (2007) 2891–2959.

[6] Y. Qin, L. Sun, X. Li, Q. Cao, H. Wang, X. Tang, L. Ye, Highly water-dispersible TiO_2 nanoparticles for doxorubicin delivery: effect of loading mode on therapeutic efficacy, Journal of Materials Chemistry 21 (2011) 18003–18010.

[7] M. Signoretto, E. Ghedini, V. Nichele, F. Pinna, V. Crocella, G. Cerrato, Effect of textural properties on the drug delivery behaviour of nanoporous TiO_2 matrices, Microporous and Mesoporous Materials 139 (2011) 189–196.

[8] S. Yamaguchi, H. Kobayashi, T. Narita, K. Kanehira, S. Sonezaki, N. Kudo, Y. Kubota, S. Terasaka, K. Houkin, Sonodynamic therapy using water–dispersed TiO_2 polyethylene glycol compound on glioma cells: Comparison of cytotoxic mechanism with photodynamic therapy, Ultrasonics Sonochemistry 18 (2011) 1197–1204.

[9] S. Naghibi, A. Jamshidi, O. Torabi, R. Ebrahimi, Application of Taguchi method for characterization of corrosion behavior of TiO_2 coating prepared by sol–gel dipping technique, International Journal of Applied Ceramic Technology (2013) http://dx.doi.org/10.1111/ijac.12077.

[10] S. Pavasupree, J. Jitputti, S. Ngamsinlapasathian, S. Yoshikawa, Hydrothermal synthesis, characterization, photocatalytic activity and dye-sensitized solar cell performance of mesoporous anatase TiO_2 nanopowders, Materials Research Bulletin 43 (2008) 149–157.

[11] M. Vijay, V. Selvarajan, K.P. Sreekumar, J. Yu, S. Liu, P. V. Ananthapadmanabhan, Characterization and visible light photocatalytic properties of nanocrystalline TiO_2 synthesized by reactive plasma processing, Solar Energy Materials and Solar Cells 9 (2009) 1540–1549.

[12] J.H. Lee, M. Kang, S.J. Choung, K. Ogino, S. Miyata, M.S. Kim, J. Y. Park, J.B. Kim, The preparation of TiO_2 nanometer photocatalyst film by a hydrothermal method and its sterilization performance for Giardia lamblia, Water Research 38 (2004) 713–719.

[13] M. Janus, A. Markowska–Szczupak, E. Kusial–Nejman, A.W. Morawski, Disinfection of E. Coli by carbon modified TiO_2 photocatalysts, Environment Protection Engineering 38 (2012) 89–97.

[14] T. Asahara, H. Koseki, T. Tsurumoto, K. Shiraishi, H. Shindo, K. Baba, H. Taoda, N. Terasaki, The bactericidal efficacy of a photocatalytic TiO_2 particle mixture with oxidizer against staphylococcus aureus, Japanese Journal of Infectious Diseases 62 (2009) 378–380.

[15] Y.H. Tsuang, J.S. Sun, Y.C. Huang, C.H. Lu, W.H. Chang, C.C. Wang., Studies of photokilling of bacteria using titanium dioxide nanoparticles, Artificial Organs 32 (2008) 167–174.

[16] T.Y. Lai, W.C. Lee, Killing of cancer cell line by photoexcitation of folic acid-modified titanium dioxide nanoparticles, Journal of Photochemistry and Photobiology A 204 (2009) 148–153.

[17] M. Song, R. Zhang, Y. Dai, F. Gao, H. Chi, G. Lv, B. Chen, X. Wang, The in vitro inhibition of multidrug resistance by combined nanoparticulate titanium dioxide and UV irradiation, Biomaterials 27 (2006) 4230–4238.

[18] Q. Li, X. Wang, X. Lu, H. Tian, H. Jiang, G. Lv, D. Guo, C. Wu, B. Chend, The incorporation of daunorubicin in cancer cells through the use of titanium dioxide whiskers, Biomaterials 30 (2009) 4708–4715.

[19] B. L'azou, J. Jorly, D. On, E. Sellier, F. Moisan, J. Fleury–Feith, J. Cambar, P. Brochard, C. Ohayon–Courtes, In vitro effects of nanoparticles on renal cells, Particle and Fibre Toxicology 5 (2008) 22–36.

[20] M.C. Hidalgo, M. Aguilar, M. Maicu, J.A. Navio, G. Colon, Hydrothermal preparation of highly photoactive TiO_2 nanoparticles, Catalysis Today 129 (2007) 50–58.

[21] G. Wang, Hydrothermal synthesis and photocatalytic activity of nanocrystalline TiO_2 powders in ethanol–water mixed solutions, Journal of Molecular Catalysis A: Chemical 274 (2007) 185.

[22] J. Zhang, X. Xiao, J. Nan, Hydrothermal-hydrolysis synthesis and photocatalytic properties of nano-TiO_2 with an adjustable crystalline structure, Journal of Hazardous Materials 176 (2010) 617–622.

[23] C. Su, C.M. Tseng, L.F. Chen, B.H. You, B.C. Hsu, S.S. Chen, Sol-hydrothermal preparation and photocatalysis of titanium dioxide, Thin Solid Films 498 (2006) 259–265.

[24] J. Liu, T. An, G. Li, N. Bao, G. Sheng, J. Fu, Preparation and characterization of highly active mesoporous TiO_2 photocatalysts by hydrothermal synthesis under weak acid conditions, Microporous and Mesoporous Materials 124 (2009) 197–203.

[25] D.S. Kim, S.Y. Kwak, The hydrothermal synthesis of mesoporous TiO_2 with high crystallinity, thermal stability, large surface area, and enhanced photocatalytic activity, Applied Catalysis A: General 323 (2007) 110–118.

[26] K. Byrappa, M. Yoshimura, Handbook of hydrothermal technology, a technology for crystal growth and materials processing, Noyes Publications, New Jersey, USA, 2001.

[27] M. Mirzaee, M.M. Amini, M. Sadeghi, F. Yeganeh Mousavi, M. Sharbatdaran, Preparation and characterization of boehmite, CuO, TiO_2, Nb_2O_5 by hydrothermal assisted sol–gel processing of metal alkoxides, Ceramics Silikaty 49 (2005) 40–47.

[28] G. Taguchi, System of experimental design, UNIPUB, Kraus International Publications, New York, USA, 1987.

[29] D.C. Montgomery, Design and analysis of experiments, 7th ed., John Wiley & Sons, New York, USA, 2009.

[30] A. Jamshidi, A.A. Nourbakhsh, S. Naghibi, K.J.D. MacKenzie, Application of the statistical Taguchi method to optimize X-SiAlON and mullite formation in composite powders prepared by the SRN process, Ceramics International (2013) http://dx.doi.org/10.1016/j.ceramint.2013.05.133.

[31] C.J. Brinker, G.W. Scherer, Sol–gel science and the physics and chemistry of sol–gel processing, Academic Press, Waltham, Massachusetts, USA, 1990.

[32] G.K. Williamson, W.H. Hall, X-ray line broadening from filed aluminium and wolfram, Acta Metallurgica 1 (1953) 22–31.

[33] X. Cao, Y. Shu, Y. Hu, G. Li, C. Liu, Integrated process of large-scale and size-controlled SnO_2 nanoparticles by hydrothermal method, Transactions of Nonferrous Metals Society of China 23 (2013) 725–730.

[34] C. Lu, C. Yeh, Infuence of hydrothermal conditions on the morphology and particle size of zinc oxide powder, Ceramics International 26 (2000) 351–357.

[35] T.D.N. Phan, H.D. Pham, T.V. Cuong, E.J. Kim, S. Kim, E.W. Shin, A simple hydrothermal preparation of TiO_2 nanomaterials using concentrated hydrochloric acid, Journal of Crystal Growth 312 (2009) 79–85.

[36] S.Y. Baek, S.Y. Chai, K.S. Hur, W.I. Lee, Synthesis of highly soluble TiO_2 nanoparticle with narrow size distribution, Bulletin of the Korean Chemical Society 26 (2005) 1333–1334.

[37] T. Sugimoto, X. Zhou, A. Muramatsu, Synthesis of uniform anatase TiO2 nanoparticles by sol–gel method, solution chemistry of $Ti(OH)_{(4-n)+n}$ complexes, Journal of Colloid and Interface Science 252 (2002) 339–346.

[38] Y.B. Ryu, W.Y. Jung, M.S. Lee, E.D. Jeong, H.G. Kim, J.S. Yang, G. D. Lee, S.S. Park, S.S. Hong, Hydrothermal synthesis of titanium dioxides from peroxotitanate solution using basic additive and their photocatalytic activity on the decomposition of orange II, Journal of Physics and Chemistry of Solids 69 (2008) 1457–1460.

[39] D.S. Kim, S.J. Han, S.Y. Kwak, Synthesis and photocatalytic activity of mesoporous TiO_2 with the surface area, crystallite size, and pore size, Journal of Colloid and Interface Science 316 (2007) 85–91.

[40] M. Zhou, J. Xu, H. Yu, S. Liu, Low-temperature hydrothermal synthesis of highly photoactive mesoporous spherical TiO_2 nanocrystalline, Journal of Physics and Chemistry of Solids 71 (2010) 507–510.

[41] C.H. Cho, M.H. Han, D.H. Kim, D.K. Kim, Morphology evolution of anatase TiO_2 nanocrystals under a hydrothermal condition (pH = 9.5) and their ultra-high photo-catalytic activity, Materials Chemistry and Physics 92 (2005) 104–111.